In Situ FTIR Measurement of Carbon Dioxide Sorption into Poly(ethylene terephthalate) at Elevated Pressures

NOEL H. BRANTLEY,* SERGEI G. KAZARIAN,† CHARLES A. ECKERT

School of Chemical Engineering and Specialty Separations Center, Georgia Institute of Technology, Atlanta, Georgia 30332

Received 20 May 1999; accepted 10 October 1999

ABSTRACT: Knowledge of the sorption rate and solubility of CO_2 in polymers are of great importance for developing technologies utilizing high-pressure and supercritical CO_2-assisted processes. Many conventional techniques for measuring gas sorption have inherent complications when used at elevated pressures. In this work, we demonstrate the use of near-IR spectroscopy as an accurate method to measure CO_2 sorption kinetics and solubility in PET at elevated pressures. Sorption kinetics and solubility are measured at 0, 28, and 50°C between pressures of 57.1 and 175.2 atm. Both initially amorphous and initially partially crystalline samples of PET are studied, and the effects of the initial crystallinity are determined. In addition, the effects of CO_2 processing on the final crystallinities of our samples are measured. Crystallization was induced in PET at 28 and 50°C over the range of pressures studied. However, at 0°C, no detectable crystallization occurred in PET, even in the presence of high pressures of CO_2. The method demonstrated in this work could easily be extended to directly measure CO_2 sorption in other polymers. © 2000 John Wiley & Sons, Inc. J Appl Polym Sci 77: 764–775, 2000

Key words: supercritical fluid; polymer; infrared spectroscopy; sorption, poly(ethylene terephthalate); diffusion; crystallization

INTRODUCTION

Compressed CO_2 as a solvent in polymer technology is of practical interest due to its environmentally benign nature, low cost, and enhancement of solute mass-transport properties in the fluid and polymer phases. For example, high-pressure and supercritical CO_2 ($scCO_2$) have been used as solvents for polymer synthesis,[1] extraction of low molecular weight compounds from polymers,[2] impregnation of polymers with chemical additives such as drugs or dyes,[3,4] formation of small uniform polymeric particles by rapid solvent expansion,[5] and creation of polymer foams.[6] Knowledge of the sorption rate and solubility of CO_2 in polymers is of great importance for developing technologies utilizing high-pressure and supercritical CO_2-assisted processes. Understanding the effects of sorbed CO_2 on the polymer properties is also vital for effective utilization of these processes. For example, to design a polymer dyeing process, the rate of dye diffusion in the polymer matrix must be known. This rate will vary directly with the free volume of the polymer, which is dependent upon the amount of CO_2 sorbed in the polymer. Thus, understanding the sorption and solubility of CO_2 and its effects on polymer free volume and dye diffusivities are crucial for design of this process. In this work, we applied *in*

Correspondence to: C. A. Eckert.
* *Present address:* Department of Chemical Engineering Imperial College, Prince Consort Road, London, UK.
† *Present address:* Albemark Process Development Center, P.O. Box 341, Baton Rouge, LA 70821.

Journal of Applied Polymer Science, Vol. 77, 764–775 (2000)

situ infrared (IR) spectroscopy in a novel manner to measure CO_2 sorption into polymers at elevated pressures.

There are three experimental techniques typically employed to determine the gas sorption in polymers at elevated pressures.[7,8] In the barometric method, the quantity of gas sorbed by a polymer sample is obtained from the difference between the amount of gas initially contacted with the polymer and the amount remaining in the gas phase after equilibration. The uptake is calculated from temperature–pressure measurements, an accurate equation of state for the gas, and calibration of the void volume of the vessel containing the polymer sample. In the gravimetric method, sorption is obtained directly from weight gain of a polymer sample as it sorbs gas and requires both an accurate balance within a pressure vessel and accounting for buoyancy effects. A less accurate alternative would be to quickly transfer the sample from a pressure vessel to an external balance. A third technique is the quartz crystal microbalance (QCM) method, in which sorption is determined from changes in the resonant frequency of a thin quartz crystal due to mass changes of well-adhered polymer coatings.

The IR spectroscopic technique that we used in this work offers the advantages of *in situ* measurement, easy operation with good accuracy, molecular level insight from spectral changes, and the ability to separate the sorption of CO_2 from other components sorbing into the polymer. The last advantage, although not employed in this work, creates the possibility to measure simultaneously the diffusion of solutes from the CO_2 fluid phase into the polymer and the sorption of the CO_2 itself into the polymer. This could not be done by any of the three previous techniques since the sorption of the multiple components is indistinguishable when calculated from the total vapor uptake or the mass of the polymer. Spectroscopic techniques other than infrared often offer this ability to study multicomponent diffusion. For example, the simultaneous diffusion of a disperse dye and liquid solvents was studied by Rutherford backscattering spectroscopy (RBS).[9]

The measurement of CO_2 sorption kinetics and solubility in semicrystalline polymers can be complicated by the additional kinetic effect of crystallization. However, there are a number of industrially important semicrystalline polymers which are candidates for CO_2 processing. For example, poly(ethylene terephthalate) (PET) is found in many textile materials where supercritical CO_2 dyeing techniques would greatly reduce water use.[10] In this work, we study the rate of CO_2 sorption in PET and the resulting effects of the sorbed CO_2 on the polymer's final degree of crystallinity. We study two separate PET samples—one which is almost completely amorphous initially and the other which has a slightly larger degree of initial crystallinity—to gain insight into the effect of the initial degree of crystallinity on sorption rates.

Crystallization will occur in the amorphous regions of a semicrystalline polymer when the operating temperature is above the glass transition temperature, T_g, and below the melting temperature, T_m, of the polymer.[11] At atmospheric conditions, crystallinity can be induced in PET thermally by heating the polymer to a temperature between its T_g of $\sim$ 70°C and its T_m of $\sim$ 270°C.[12] Upon heating a semicrystalline polymer above its T_g, there is a sharp increase in the mobility of the polymer chains which allows the chains to rearrange into the crystalline state.

An alternative to increasing the operating temperature above T_g to induce crystallization is to reduce T_g below the operating temperature of the system, as by sorbing a gas in the polymer. Glass transition temperatures for PET containing dissolved CO_2 at elevated pressures were estimated by Chiou et al. using differential scanning calorimetry (DSC).[13,14] The glass transition temperatures were found to be 35°C at 35 atm and 52°C at 20 atm. Mensitieri et al. applied conventional and high-pressure DSC to study and confirm the reduction of T_g when PET was exposed to CO_2 at up to 50 atm and 50°C.[15] Previous studies showed that the T_g depression is proportional to the amount of CO_2 sorbed. Thus, crystallization occurs only when the amount of sorbed CO_2 is enough to reduce T_g below the operating temperature.[8,16–18]

Crystallization and sorption kinetics have been shown to increase with pressure between 40 and 60 atm for an operating temperature of 35°C.[19] Also, the solubility of CO_2 in PET has been shown to decrease with increasing temperature between 35 and 65°C for a given pressure of 50 atm.[20] In these and other previous studies, the sorption and solubility have only been studied near or above ambient temperatures. At these temperatures, crystallization has been observed when using only modest pressures of CO_2. In this work, we investigated the effect of temperature, including below ambient, at high and low pressures on the

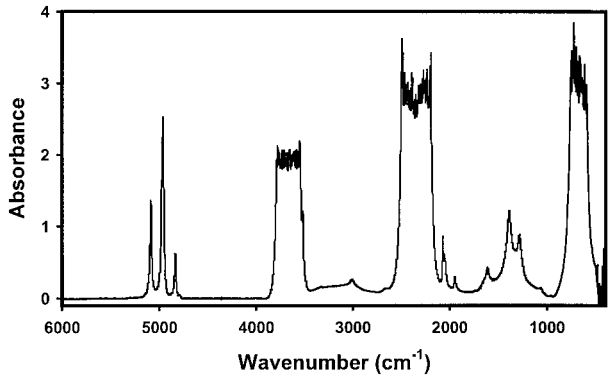

Figure 1 IR spectra of CO_2 at 50°C and 174.0 atm (0.749 g/cm^3) in a high-pressure cell having a path length of 5.9 mm. The NIR $\nu_1 + 2\nu_2^0 + \nu_3$ vibration, centered at 4966 cm^{-1}, is used in this study to quantify the concentration of CO_2 in PET.

sorption kinetics and solubility of CO_2 into PET. T_g may not be reduced enough to induce crystallization in PET when operating at below ambient conditions even with moderate to high pressures of CO_2. Therefore, we also studied the effects of CO_2 sorption on the resulting crystallinity of the polymer.

EXPERIMENTAL

Materials

SFC-grade carbon dioxide (99.99% purity) was purchased from Matheson (Montgomeryville, PA 18936). The CO_2 was passed over a Matheson Type 451 molecular sieve gas purifier prior to use to remove trace water and hydrocarbons. Amorphous and partially crystalline PET films were obtained from the E. I. DuPont Co. through the courtesy of Dr. Fenghua Deng. The amorphous and partially crystalline films were 1.0- and 1.5-mm thick, respectively, as reported by the supplier and verified by measurement with calipers. Initial crystallinities were measured to be 2.5 ± 0.5% for the amorphous PET and 6.1 ± 1.0% for the partially crystalline PET. Since the degree of crystallinity is very small in the amorphous samples, we will refer to these samples as "initially amorphous PET." The 6.1% crystalline samples will be referred to as "initially partially crystalline PET."

In Situ FTIR Spectroscopy

We studied the diffusion of CO_2 into PET by an *in situ* transmission near-IR (NIR) spectroscopic method which allowed direct measurement of the CO_2 concentration within the polymer without disturbing the polymer. Traditional mid-IR (MIR) spectroscopy has proven its usefulness for quantifying solute concentrations in the polymer and fluid[21–23] and has, in fact, been applied to measure the solubility and sorption of CO_2 in polymers at pressures below 5 atm.[24,25] In addition to measurement of concentrations, traditional MIR spectroscopy is a valuable tool for studying the effects of the dissolved fluid on the polymer[23,26,27] and specific interactions of CO_2 with polymers.[28] The ability to gain molecular level insight, and, thus, a molecular basis for understanding macroscopic phenomena such as gas solubilities, is a major advantage of IR spectroscopy over other techniques.

One obstacle to applying transmission MIR spectroscopy to study high-pressure systems is the very large absorbances arising from the dense fluid phase. For example, Figure 1 shows an infrared spectra of CO_2 at 50°C and 174.0 atm, which corresponds to a CO_2 density of 0.749 g/cm^3, in a high-pressure cell having a path length of 5.9 mm. The CO_2 absorbances centered at approximately 3750, 2300, and 750 cm^{-1} are offscale, indicating that essentially all of the IR radiation in these regions is completely absorbed by the dense CO_2, rendering these regions useless for quantification. Our experiments have the added complication of strong PET absorbances in the mid-IR (4000–400 cm^{-1}), as shown in Figure 2. These strong or offscale regions block most of the weaker CO_2 absorbances which we considered to use for measurement of sorption.

To overcome complications due to strong MIR absorbance of CO_2, researchers have employed

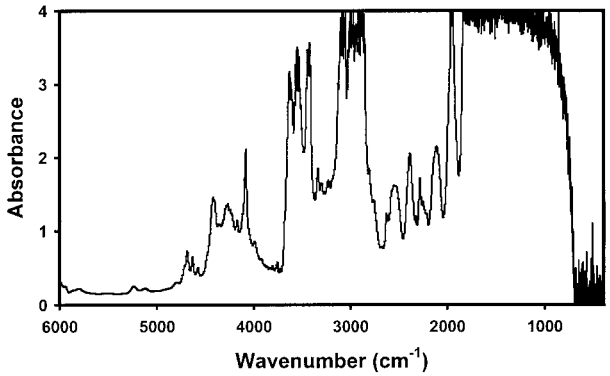

Figure 2 IR spectra of 1.0-mm-thick amorphous PET film. The polymer is nearly transparent in the NIR above 4800 cm^{-1}.

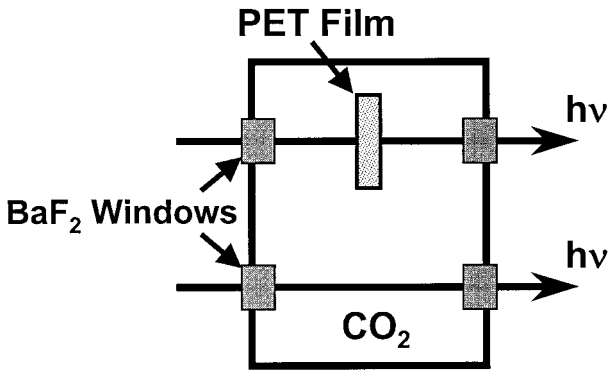

Figure 3 Schematic of the high-pressure cell used in this work. The cell contains two parallel optical paths and was equipped with BaF_2 windows. A polymer film is secured in one optical path and the cell pressurized with CO_2 to start a sorption experiment.

methods such as using deuterated compounds to shift IR absorbances,[21,22] applying attenuated total reflectance IR (ATR–IR) techniques,[28] and looking in the NIR region (>4000 cm^{-1}) where CO_2 and many other fluids are much more transparent.[29] Using deuterated compounds is not an option in our work. ATR–IR is also not suitable for our measurements since the validity of Beer's law is much harder to prove under the conditions of *in situ* ATR–IR. The third alternative of looking in the near-IR proved very useful for our experiments. As shown in Figure 2, there is very little PET absorbance above 4700 cm^{-1}. In addition, the spectra in Figure 1 show that CO_2 has three absorbances in the near-IR which are fairly intense but remain onscale and therefore useful. These absorbances centered at 5088, 4966, and 4837 cm^{-1} are due to the $2\nu_1 + \nu_3$, $\nu_1 + 2\nu_2^0 + \nu_3$, $4\nu_2^0 + \nu_3$ Fermi triad.[30] The $\nu_1 + 2\nu_2^0 + \nu_3$ absorbance, which was the most intense of the three, was used in this work for measuring the CO_2 sorption in PET. The ν_1 and ν_3 fundamental modes provide most of the intensity of this band, while the $2\nu_2^0$ provides a shift of this absorption that allows separation of CO_2 in the polymer matrix from that in the gaseous state, which will be discussed later.

Apparatus

A schematic of the high-pressure optical cell used in this study is shown in Figure 3. This cell contains two parallel optical paths that allow measurement of the polymer phase and the fluid phase spectra separately under identical conditions. Details about the construction of this cell can be found elsewhere.[31] A magnetic stir bar was used to ensure uniform conditions within the cell. All spectra were taken on a Bruker 66ν/s FTIR vacuum spectrometer, configured for the mid-IR region with a globar source, a KBr beam splitter, and a DTGS detector, with a resolution of 2 cm^{-1}. Spectral analysis were performed on the Opus software controlling the Bruker spectrometer. Temperatures above ambient were controlled with Omega cartridge heaters connected to an Omega CN9000a temperature controller. Below ambient, the temperature was maintained by flowing chilled ethylene glycol from a Neslab Model RTE-210 temperature bath through a custom built aluminum jacket which surrounded the cell without blocking the optical paths. CO_2 was added to the cell using an ISCO 260D syringe pump, and system pressure was measured with a Heise DPI 260 3000 psi pressure gauge. A small electric fan blowing across a slightly warm hot plate was used to pass a stream of warm air over the optical windows of the cell at 0°C. This was done to prevent precipitation of water vapor on the windows, which would interfere with the IR measurements.

CO_2 Sorption Measurements

The conditions for CO_2 sorption measured in this work are shown in Tables I and II for the initially amorphous and partially crystalline PET, respec-

Table I Conditions and Final PET Crystallinity After Processing of Initially Amorphous PET

Temperature (°C)	Pressure (atm)	CO_2 Density (g/cm^3)	Final PET Crystallinity	Diffusivity (cm^2/s)
0	63.0	0.952	2.5% ± 0.5%	1.2×10^{-8}
28	175.2	0.884	23.1% ± 0.7%	8.2×10^{-8}
28	54.2	0.149	20.8% ± 0.8%	5.4×10^{-8}
50	171.7	0.749	27.6% ± 0.6%	2.2×10^{-7}
50	61.2	0.142	25.8% ± 0.6%	1.8×10^{-7}

Table II Conditions and Final PET Crystallinity After Processing of Initially Semicrystalline PET

Temperature (°C)	Pressure (atm)	CO_2 Density (g/cm^3)	Final PET Crystallinity	Diffusivity (cm^2/s)
0	65.2	0.953	6.2% ± 1.0%	1.3×10^{-8}
28	172.3	0.882	22.7% ± 1.0%	7.1×10^{-8}
28	57.1	0.165	21.8% ± 0.8%	5.5×10^{-8}
50	174.5	0.753	27.3% ± 0.5%	2.0×10^{-7}
50	61.2	0.142	24.3% ± 0.5%	1.5×10^{-7}

tively. The CO_2 densities shown in these tables were calculated with the 32-parameter modified Benedict–Webb–Rubin equation of state.[32] The pressures were chosen so that not greatly dissimilar CO_2 densities would be studied for the three temperatures of 0, 28, and 50°C. Sorption experiments were performed as follows: A slab of PET film approximately 1 × 1.5 in. was placed in one optical path of the cell which had a path length of 0.289 cm. After sealing, the high-pressure cell was heated or cooled to the desired temperature. The cell was typically evacuated overnight to remove residual water. A sorption isotherm was initialized by adding CO_2 to the system until the desired pressure was obtained, and then the cell was sealed. The cell volume was large enough (ca. 40 mL) that any decrease in pressure due to CO_2 sorption into the polymer was less than the experimental uncertainty in our pressure measurement (ca. ±1%). CO_2 addition typically took less than 2 min, resulting in negligible error to the initial time, t_0, since the time scale of the sorption experiments was hours to days. Spectra were taken through the polymer path at regular time intervals during the course of the experiment.

Figure 4 shows a sample of the spectroscopic data recorded during one of our sorption experiments (1.0 mm amorphous PET, 50°C, and 174.0 bar). From this figure, we see a shoulder appear and grow with time on the lower-energy side of the $\nu_1 + 2\nu_2^0 + \nu_3$ vibration of CO_2. Subtraction of the initial spectra, in which there is no CO_2 in the polymer, removes the contribution of the fluid phase CO_2. The spectral subtraction reveals a new absorption band, as shown in Figure 5. This band, which is shifted to lower energy, is the $\nu_1 + 2\nu_2^0 + \nu_3$ of the CO_2 *within* the polymer. The $2\nu_2^0$ bending mode vibration of CO_2 is responsible for the spectra shift, since this vibration has been shown to shift in frequency as a result of interaction of the CO_2 molecules with polymer matrices.[28]

Molar Absorptivity of CO_2

Concentrations of CO_2 in the polymer are determined from the measured infrared intensities of the $\nu_1 + 2\nu_2^0 + \nu_3$ vibration by the Beer–Lambert law given below:

$$A = \varepsilon c l \tag{1}$$

where A is the absorbance; ε, the molar absorptivity; c, the concentration of CO_2; and l, the path length. Since the path length is known, only the molar absorptivity is required. The molar absorptivity of the $\nu_1 + 2\nu_2^0 + \nu_3$ spectral band used in this work has been shown to be independent of temperature over the range of 27 to 227°C and independent of CO_2 density up to about 0.9 g/cm^3.[30] Our experiments fall within this CO_2 density range, and based on the large range of temperature independence, we make the assump-

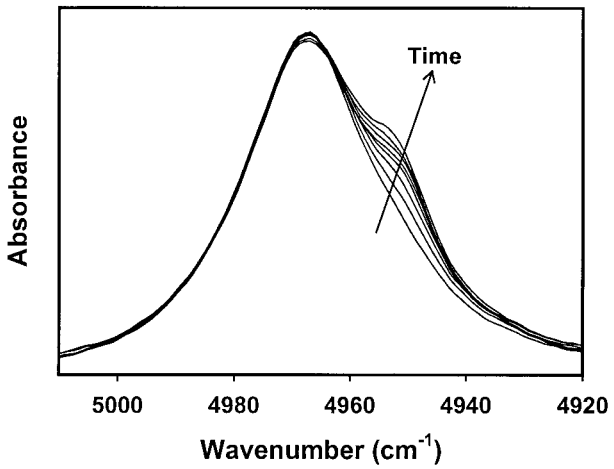

Figure 4 IR spectra of the $\nu_1 + 2\nu_2^0 + \nu_3$ vibration of CO_2 measured during a sorption experiment at 50°C and 174.0 bar. The shoulder is due to CO_2 *within* the polymer and is shifted to a lower wavenumber due to interactions of the CO_2 with PET. The intensity of the shoulder increases with time.

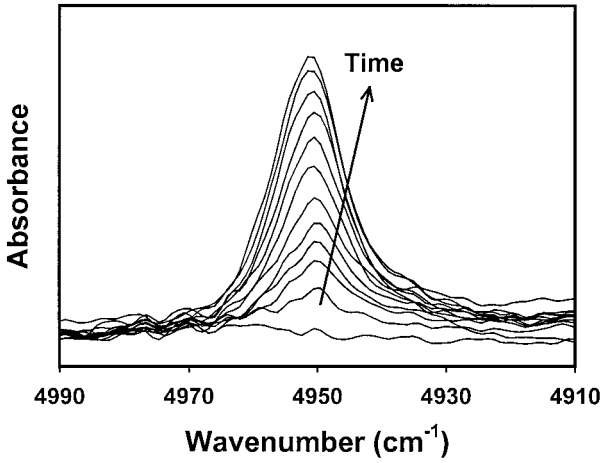

Figure 5 Results of subtracting the spectra of fluid CO_2, taken at time = 0, from subsequent spectra. The spectral subtraction reveals the $\nu_1 + 2\nu_2^0 + \nu_3$ vibration of CO_2 within PET. The intensity of this band is used to calculate the concentration of CO_2 in the polymer.

tion that the molar absorptivity will remain independent of temperature down to our lowest temperature of 0°C. In addition, since the molar absorptivity of this vibrational band has very little dependence on the surrounding environment, we assume that the value in the polymer is equivalent to the value in the fluid phase.

It should be noted that the molar absorptivity of CO_2 is not necessary to calculate a diffusion profile from the spectral absorbances measured. Since the molar absorptivity is constant during a sorption experiment, the ratio of CO_2 absorbance at any given time to the maximum CO_2 absorbance during the sorption experiment is proportional to the relative mass uptake of CO_2 at the given time to the mass uptake when the CO_2 absorbance is maximum. The relative mass uptake provides a description of the mechanism of diffusion,[33] which will be further discussed later.

Crystallinity Measurements

The degree of crystallinity of our PET samples before and after sorption experiments was estimated by relating the degree of crystallinity to the bulk polymer density. This technique assumes that (1) the polymer is a two-phase system consisting of an amorphous or glassy phase in which ordered crystal-like regimes are embedded on a microscopic scale, (2) the amorphous and crystalline phases have well-characterized densities (ρ_a and ρ_c, respectively), and (3) the bulk polymer density can be expressed as

$$\rho = (1 - x_c)\rho_a + x_c\rho_c \quad (2)$$

where x_c is the volume fraction of the crystalline phase.[19] Values of 1.331 and 1.455 g/mL were used for the density of amorphous and crystalline PET, respectively.[16] Polymer density measurements were most kindly made for us by Nadim Qureshi at Case Western University and by Kip Sturgill at Georgia Tech utilizing density gradient columns calibrated with glass floats of known density.

RESULTS AND DISCUSSION

Effect of CO_2 Sorption on Crystallinity

The amorphous and partially crystalline PET samples used in this study were determined to have pretreatment crystallinities of 2.5 ± 0.5% and 6.1 ± 1.0%, respectively, by the density gradient column technique. The posttreatment crystallinities of the initially amorphous and the initially partially crystalline PET samples are listed in Tables I and II, respectively. From these tables, we see that CO_2 sorption at 28 and 50°C induced crystallization in the polymer, whereas at 0°C, no detectable crystallization occurred in PET. Evidently, at 0°C, the mobility of the polymer chains was not enough, even in the presence of CO_2, to allow reorientation into the thermodynamically favorable crystalline state.

We must note that CO_2-induced crystallization in a polymer may result in a slightly different morphology than will crystallization by heat or stress. For example, the effect of CO_2 on PET morphology has been studied via wide-angle X-ray scattering and scanning electron microscopy where differences in size and orientation of crystallites were observed.[34] Vibrational spectroscopy,[35] NMR,[36] and DSC[37] also serve as premier tools for studying the effects of CO_2 on the microstructure of polymers such as PET. Investigation of the microscopic and molecular level differences between heat- or stress-induced crystallization and CO_2-induced crystallization has been discussed previously.

CO_2 Sorption into PET

The results of the CO_2-sorption experiments at pressures corresponding to densities of CO_2 in the range of 0.749–0.953 g/cm^3 are shown in Figures 6 and 7 for the initially amorphous and partially

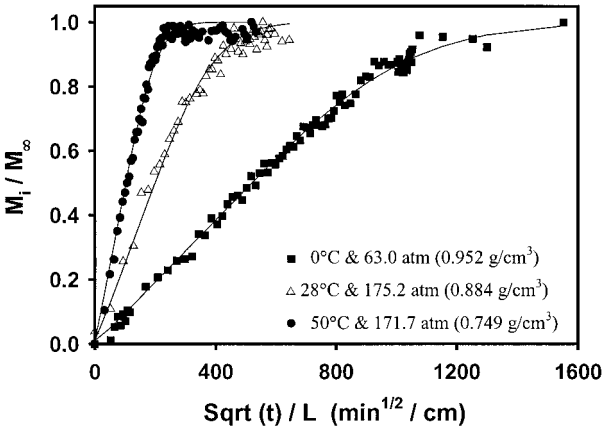

Figure 6 Relative mass uptake of CO_2 into initially amorphous PET. The values in parentheses indicate the calculated density of the CO_2 phase. The solid lines are fits of the sorption isotherms to a Fickian model. Increasing temperature at a not greatly dissimilar CO_2 density increased the rate of CO_2 sorption in the polymer.

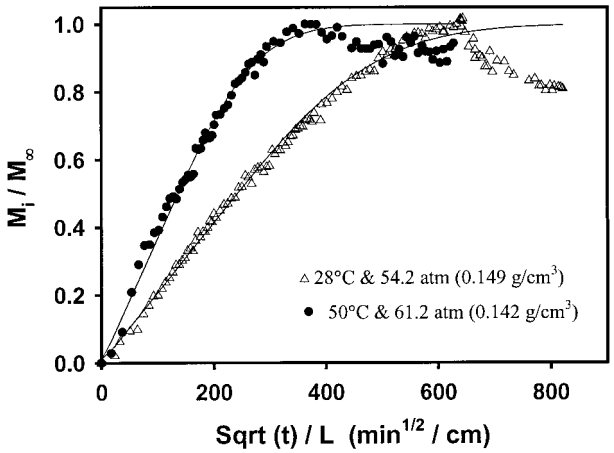

Figure 8 Relative mass uptake of CO_2 into initially amorphous PET. The values in parentheses indicate the calculated density of the CO_2 phase. The solid lines are fits of the sorption isotherms to a Fickian model. These data clearly show a maximum uptake of CO_2 and subsequent decrease in CO_2 concentration due to induced crystallization.

crystalline PET, respectively. Figures 8 and 9 show the results at pressures corresponding to densities of CO_2 in the range of 0.142–0.165 g/cm^3 for the initially amorphous and partially crystalline PET, respectively. The ordinate is the relative mass uptake of CO_2 at any given time, M_i, divided by the maximum mass uptake, M_∞, and the abscissa is the square root of time divided by the unswollen polymer thickness. This time scale was chosen because the initial (linear) slope of the sorption curve can be related directly to the diffusivity of the solvent in the polymer if Fickian diffusion applies.[33] Dividing the time scale by polymer thickness also allowed comparison of samples which had different thicknesses. Using the unswollen polymer thickness introduced negligible error in our results, since, at our experi-

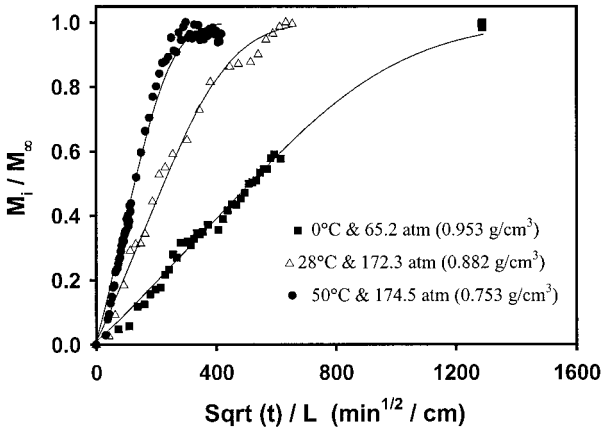

Figure 7 Relative mass uptake of CO_2 into initially partially crystalline PET. The values in parentheses indicate the calculated density of the CO_2 phase. The solid lines are fits of the sorption isotherms to a Fickian model. Again, increasing temperature at a nearly constant CO_2 density increases the rate of CO_2 sorption in the polymer.

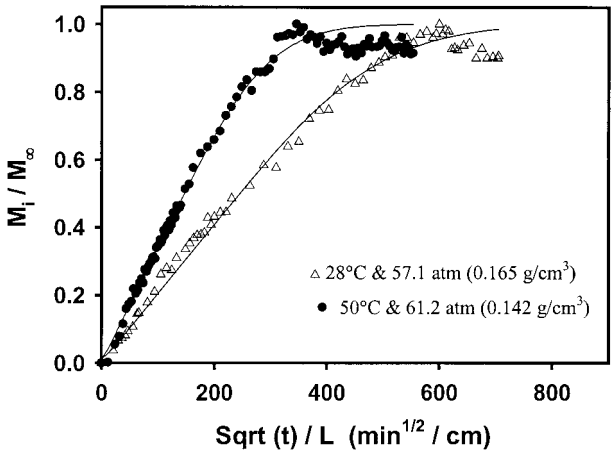

Figure 9 Relative mass uptake of CO_2 into initially partially crystalline PET. The values in parentheses indicate the calculated density of the CO_2 phase. The solid lines are fits of the sorption isotherms to a Fickian model. Again, the data clearly show a maximum uptake of CO_2 and subsequent decrease in CO_2 concentration due to induced crystallization.

mental conditions, PET has been shown to increase in volume by less than 2%.[38]

Figures 6–9 show that the rate of CO_2 sorption into PET increases with increasing temperature for not greatly dissimilar fluid densities, as indicated by the increasing initial slopes of the sorption curves with temperature. This was expected since the rate of CO_2 sorption is dependent upon polymer plasticization, which increases with temperature. We also see that the rate of CO_2 sorption was higher at higher pressure for a given temperature. This is consistent with literature results and was expected since the driving force for sorption is directly proportional to fluid density at a given temperature.

A maximum in the amount of CO_2 sorbed in the PET was observed as a function of time for the 28 and 50°C isotherms in both the amorphous and partially crystalline samples and at low and high CO_2 density. The subsequent decrease in CO_2 solubility is attributed to crystallization of the initially amorphous regions of the polymer samples. Crystallization does not occur until enough CO_2 has sorbed into the polymer to reduce its glass transition temperature below the operating temperature. As crystallization occurs, the bulk CO_2 concentration decreases as a result of the lack of solubility of CO_2 in the crystalline regions of PET. We did not observe a maximum in the amount of CO_2 sorbed in PET at 0°C, which is consistent with the polymer density results indicating that PET does not crystallize at this temperature.

A comparison of relative sorption results for the initially amorphous and partially crystalline PET samples at an individual temperature and pressure reveals that the sorption curves are nearly identical. An example of this is shown in Figure 10 for the conditions of 28°C and 54.2 atm for the initially amorphous PET and 57.1 atm for the partially crystalline PET. Since the relative mass uptake is indicative of the mechanism of diffusion, this result suggests that the presence of approximately 3.4% more crystalline structure in PET does not significantly alter the mechanism for diffusion of CO_2. Considering that CO_2 diffusion will occur only in the amorphous regions of PET, we conclude that there is little difference in the resistance to mass transfer in the amorphous regions of PET for our two samples at all conditions studied.

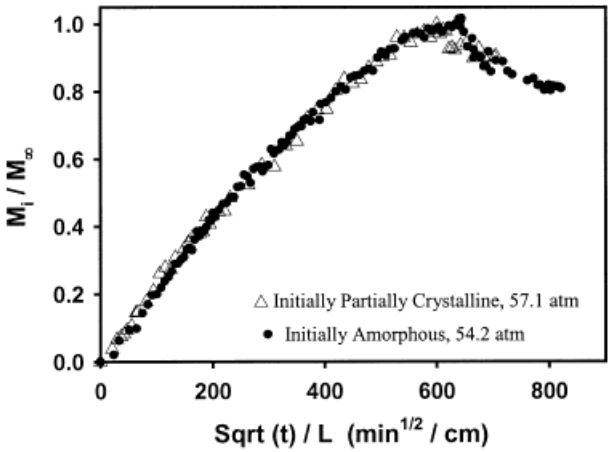

Figure 10 Comparison of the effect of initial polymer crystallinity on the relative mass uptake of CO_2 into PET at 28°C. The initial polymer crystallinity had little effect on the relative mass uptake of CO_2 into PET.

Diffusivity of CO_2 in Amorphous PET

Diffusivities of CO_2 in amorphous PET were calculated from the initial slopes of the sorption curves by fitting our data the following Fickian model which describes one-dimensional diffusion of a component through a finite plate[33]:

$$\frac{M_t}{M_\infty} = 1 - \sum_{n=0}^{\infty} \frac{8}{(2n+1)^2\pi^2} \exp\left[-\frac{D(2n+1)^2\pi^2 t}{4l^2}\right] \tag{3}$$

where D is the diffusivity; l, the thickness of the film; and t, the time. Fits of the initial slopes of our data are shown as solid lines in Figures 6–9. We see that this model fits our data well at times below the maximum in CO_2 sorption, consistent with a Fickian mechanism of CO_2 diffusion through the amorphous regions of PET. Calculated diffusivities for CO_2 in amorphous PET for all our experiments are given in Tables I and II for the initially amorphous and partially crystalline samples, respectively. Lambert and Paulaitis estimated the diffusivity of CO_2 into PET at 35°C and 60 atm to be 4.2×10^{-8} cm^2/s, which is in reasonable agreement with the results obtained in this work at 28°C and similar pressures.[19]

It is important to note that the diffusivity calculated from eq. (3) above is sensitive to the value of sample thickness used in the calculation. For example, a 10% change in the polymer thickness measurement results in a 21% change in the calculated diffusivity for our sorption into initially amorphous PET at 50°C and high CO_2 density. Errors due to inaccurate polymer thickness were minimized in this work by verifying the polymer

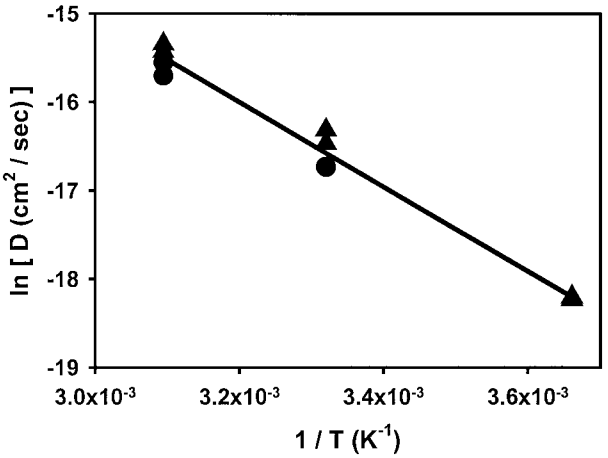

Figure 11 Arrhenius plot of the temperature dependence of the diffusivity of CO_2 in amorphous PET. (●) Data at high CO_2 fluid densities; (▲) data at low CO_2 fluid densities. The solid line is a fit of all data, giving an Arrhenius activation energy of $4.0 \times 10^4 \pm 0.7 \times 10^4$ J/mol.

thickness reported by the manufacturer with calipers and noting that PET swelling by CO_2 has a very small effect (on the order of 1%) on polymer thickness at the conditions studied.

With the temperature dependence of the diffusivity at both low and high CO_2 density, we then calculated an Arrhenius activation energy according to

$$D = D_0 e^{-E/RT} \tag{4}$$

where D_0 is a temperature-independent constant, and E, the Arrhenius activation energy. Figure 11 is a plot of $\ln(D)$ versus $1/T$. The slope of the linear fit of our data is used to calculate E for CO_2 sorption in amorphous PET, which resulted in $E = 4.0 \times 10^4 \pm 0.7 \times 10^4$ J/mol (regression $r^2 = 0.980$). For comparison, the activation energy was calculated from CO_2 diffusion data reported by Hirose et al. for pressures less than 1 atm and similar temperatures studied in this work.[39] Their data gave $E = 4.4 \times 10^4$ J/mol, indicating consistency between the two studies.

CO_2 Molar Absorptivity

We calibrated the molar absorptivity of the $\nu_1 + 2\nu_2^0 + \nu_3$ vibrational band by measuring the fluid spectra of CO_2 through a known path length at the temperatures used in this study and over a range of densities. The Peng–Robinson equation of state was used to calculate the CO_2 density from temperature and pressure data. Figure 12 shows a plot of the absorbance of this vibration divided by the cell path length is shown as a function of concentration. The data at 0, 28, and 50°C all fall on a single straight line, indicating that the Lambert–Beer law is indeed obeyed, and the molar absorptivity of this band is essentially independent of temperature and CO_2 density for the range of conditions that we studied. From the slope of this line, the molar absorptivity of this band was determined to be 6.4 L mol^{-1} cm^{-1}.

Solubility of CO_2 in PET

The molar absorptivity of CO_2 was then used to calculate the concentration of CO_2 in the polymer both during sorption and at equilibrium from the absorbance data presented earlier. The density of PET is necessary to convert the CO_2 concentrations to mass fraction CO_2 in the polymer. The density changes as the polymer crystallizes, however, and we do not know the exact PET density at all experimental times. Fortunately, the difference in polymer density between the totally amorphous and semicrystalline PET is small. Thus, we assume a constant density for PET equal to 1.35 g/cm^3 when calculating the mass fraction of CO_2 in the polymer. This assumption should introduce a negligible 1.5% error or less in our mass fraction calculations.

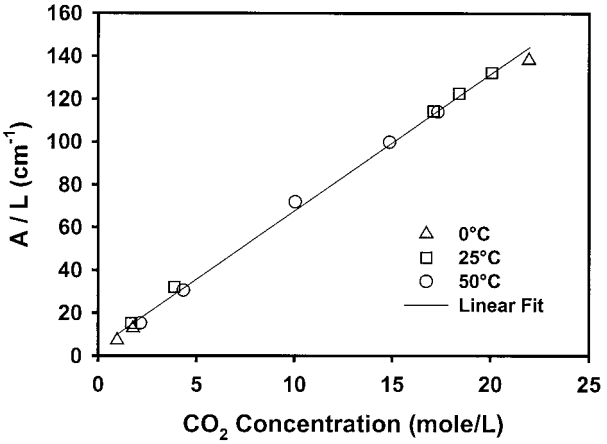

Figure 12 Plot of the IR absorbance of the $\nu_1 + 2\nu_2^0 + \nu_3$ vibrational band of CO_2 divided by the path length versus CO_2 concentration. The linearity of the data indicates validity of the Beer–Lambert law over the range of CO_2 concentrations and temperatures used in this study. From the fitted slope of the data, the molar absorptivity of this band was determined to be 6.4 L mol^{-1} cm^{-1}.

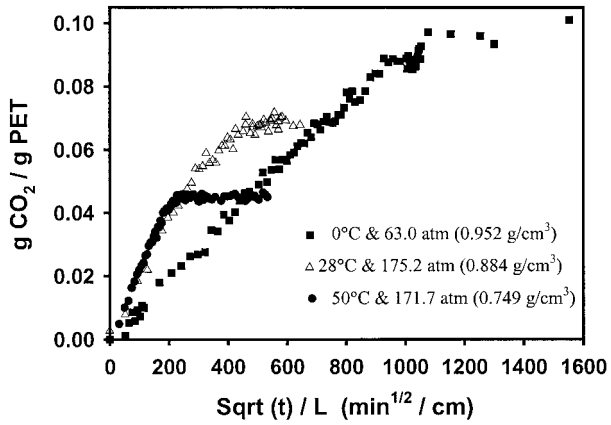

Figure 13 Sorption kinetics and solubility of CO_2 in initially amorphous PET. High-density fluid CO_2 results.

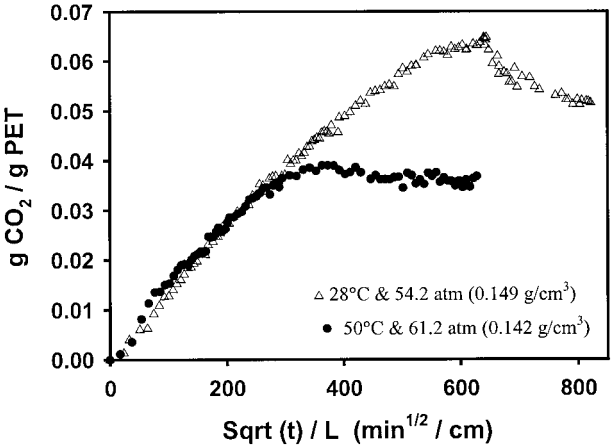

Figure 15 Sorption kinetics and solubility of CO_2 in initially amorphous PET. Low-density fluid CO_2 results.

Figures 13 and 14 show our results in terms of mass CO_2 per mass of PET for initially amorphous and partially crystalline polymer, respectively, at pressures corresponding to high CO_2 density. Figures 15 and 16 show the mass fraction results at pressures corresponding to low CO_2 density for the initially amorphous and partially crystalline PET, respectively. A comparison of the maximum CO_2 solubility (C_{max}) obtained in this work to values reported by Lambert and Paulaitis and Kamiya et al. at similar conditions are shown in Table III. These data are for CO_2 sorption into amorphous PET. The agreement of the data validate the accuracy our technique.

Our results show a decrease in CO_2 equilibrium solubility in PET with increasing temperature over the range of 0–50°C. Similar decreases in solubility were observed by Kamiya et al.[20] upon increasing temperature from 35 to 65°C at pressures up to 50 atm and by Hirose et al.[39] upon increasing temperature from 25 to 65°C at pressures up to 1 atm. Spectroscopic evidence has shown the existence of a specific interaction between CO_2 and various polymers[28] and confirmed by recent *ab initio* calculations for PET.[40] This interaction is exothermic in nature, which explains the decrease in CO_2 solubility with an increase in temperature. Our results also show that the solubility of CO_2 in PET is larger at higher pressure for the same temperature. This trend was observed by Lambert and Paulaitis at 35°C.[19] The initial crystallinity of our polymer had no

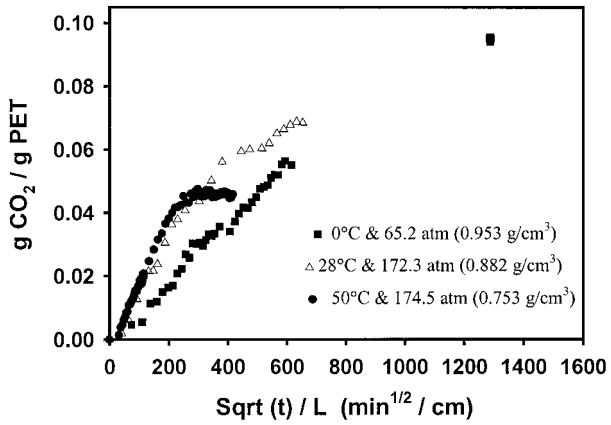

Figure 14 Sorption kinetics and solubility of CO_2 in initially partially crystalline PET. High-density fluid CO_2 results.

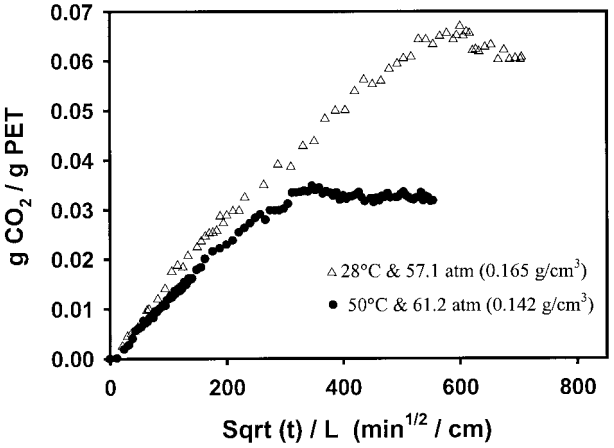

Figure 16 Sorption kinetics and solubility of CO_2 in initially partially crystalline PET. Low-density fluid CO_2 results.

Table III Comparison of Maximum CO_2 Concentrations in Amorphous PET Measured in This Work to Literature Values

	Temperature (°C)	Pressure (atm)	C_{max} (g CO_2 per g polymer)
This study	28	54.2	0.0648
Lambert and Paulaitis[19]	35	50	0.0651
Kamiya et al.[20]	35	50	0.0644

significant influence on the maximum solubility of CO_2 in PET at 28 and 50°C. This is likely due to induced crystallinity in the polymer, resulting in the two samples having similar crystallinities nearing maximum CO_2 solubility. At 0°C, the solubility of CO_2 was observed to be slightly higher ($\sim$ 5%) in amorphous PET samples versus the partially crystalline PET ones, which can be attributed to the larger amount of amorphous volume in the less crystalline PET.

CONCLUSIONS

We utilized *in situ* NIR spectroscopy in a novel manner to measure sorption isotherms of CO_2 in PET. This method offers advantages over a number of conventional techniques for measuring CO_2 sorption at high pressures or fluid densities. Comparison of our results to the literature verified the accuracy of this method, and this method could easily be extended to studying CO_2 concentrations in other polymers.

Diffusivities of CO_2 in amorphous PET were determined from a Fickian fit of the initial slopes of the sorption isotherms. The diffusivity increases with increasing temperature, with an Arrhenius activation energy of $4.0 \times 10^4 \pm 0.7 \times 10^4$ J/mol. The equilibrium solubility of CO_2 was shown to decrease with increasing temperature for the conditions of this study. The initial crystallinity of the PET studied in this work had no significant effect on the sorption kinetics and solubility of CO_2 in the polymer at 28 and 50°C, but had a small effect ($\sim$ 5%) at 0°C. We have also shown that CO_2 sorption into amorphous PET at 28 and 50°C induces crystallinity in the polymer, whereas sorption at 0°C did not induce crystallinity within our time frame.

REFERENCES

1. Kendall, J. L.; Canelas, D. A.; Young, J. L.; DeSimone, J. M. Chem Rev 1999, 99, 543.
2. McHugh, M. A.; Krukonis, V. J. Supercritical Fluid Extraction—Principles and Practice, 2nd ed.; Butterworths-Heinemann: Boston, 1994.
3. West, B. L.; Kazarian, S. G.; Vincent, M. F.; Brantley, N. H.; Eckert, C. A. J Appl Polym Sci 1998, 69, 911.
4. Berens, A. R.; Huvard, G. S.; Korsmeyer, R. W.; Kunig, F. W. J Appl Polym Sci 1992, 46, 231.
5. Dixon, D. J.; Luna-Barcenas, G.; Johnston, K. P. Polymer 1994, 35, 3998.
6. Kumar, V.; Gebizioglu, O. S. In Annual Technical Conference ANTEC Conferences Proceedings Montreal, Quebec, 1991; p 1297.
7. Aubert, J. H. J Supercrit Fluids 1998, 11, 163.
8. Wissinger, R. G.; Paulaitis, M. E. J Polym Sci B Polym Phys Ed 1987, 25, 2497.
9. Stinson, R. M.; Obendorf, S. K. J Appl Polym Sci 1996, 62, 2121.
10. Chang, K. H.; Bae, H. K.; Shim, J. J. Kor J Chem Eng 1996, 13, 310.
11. Beckman, E. J.; Porter, R. S. J Polym Sci B Polym Phys Ed 1987, 25, 1511.
12. Cobbs, W. H.; Burton, R. L. J Polym Sci 1953, 10, 275.
13. Chiou, J. S.; Barlow, J. W.; Paul, D. R. J Appl Polym Sci 1985, 30, 3911.
14. Chiou, J. S.; Barlow, J. W.; Paul, D. R. J Appl Polym Sci 1985, 30, 2633.
15. Mensitieri, G.; Nobile, M. A. D.; Guerra, G.; Apicella, A.; Ghatta, H. A. Polym Eng Sci 1995, 35, 506.
16. Michaels, A. S.; Vieth, W. R.; Barrie, J. A. J Appl Phys 1963, 34, 1.
17. Michaels, A. S.; Vieth, W. R.; Barrie, J. A. J Appl Phys 1963, 34, 13.
18. Mizoguchi, K.; Hirose, T.; Naito, Y.; Kamiya, Y. Polymer 1987, 28, 1298.
19. Lambert, S. M.; Paulaitis, M. E. J Supercrit Fluids 1991, 4, 15.
20. Kamiya, Y.; Hirose, T.; Naito, Y.; Mizoguchi, K. J Polym Sci B Polym Phys Ed 1988, 25, 159.
21. Vincent, M. F.; Kazarian, S. G.; Eckert, C. A. AIChE J 1997, 40, 1838.
22. Vincent, M. F.; Kazarian, S. G.; West, B. L.; Berkner, J. A.; Bright, F. V.; Liotta, C. L.; Eckert, C. A. J Phys Chem B 1998, 102, 2176.
23. Kazarian, S. G.; Brantley, N. H.; Eckert, C. A. CHEMTECH 1999, 29(7), 36.
24. Brolly, J. B.; Bower, D. I.; Ward, I. M. J Polym Sci B Polym Phys 1996, 34, 769.

25. Webb, J. A.; Bower, D. I.; Ward, I. M.; Cardew, P. T. Polymer 1992, 33, 1321.
26. Fried, J. R.; Li, W. J Appl Polym Sci 1990, 41, 1123.
27. Kazarian, S. G.; Brantley, N. H.; West, B. L.; Vincent, M. F.; Eckert, C. A. Appl Spectrosc 1997, 51, 491.
28. Kazarian, S. G.; Vincent, M. F.; Bright, F. V.; Liotta, C. L.; Eckert, C. A. J Am Chem Soc 1996, 118, 1729.
29. Swaid, I.; Nickel, D.; Schneider, G. M. Fluid Phase Equilibr 1985, 21, 95.
30. Buback, M. In Supercritical Fluids: Fundamentals for Application; Kiran, E.; Sengers, J. M. H. L., Eds.; Kluwer: Dordrecht, 1994; p 499.
31. Kazarian, S. G.; Vincent, M. F.; Eckert, C. A. Rev Sci Instrum 1996, 67, 1586.
32. Ely, J. F.; Haynes, W. M.; Bain, B. C. J Chem Thermodyn 1989, 21, 879.
33. Crank, J. The Mathematics of Diffusion; Clarendon: Oxford, 1975.
34. Sfiligoj, M. S.; Zipper, P. Colloid Polym Sci 1998, 276, 144.
35. Kazarian, S. G.; Brantley, N. H.; Eckert, C. A. Vibra Spectrosc 1999, 19, 277.
36. Bai, S.; Hu, J. Z.; Pugmire, R. J.; Grant, D. M.; Taylor, C. M. V.; Rubin, J. B.; Peterson, E. J. Macromolecules 1998, 31, 9238.
37. Zhong, Z.; Zheng, S.; Mi, Y. Polymer 1999, 40, 3829.
38. Chang, S. H.; Park, S. C.; Shim, J. J. J Supercrit Fluids 1998, 13, 113.
39. Hirose, T.; Mizoguchi, K.; Kamiya, Y.; Terada, K. J Appl Polym Sci 1989, 37, 1513.
40. Nelson, M. R.; Borkman, R. F. J Phys Chem A 1998, 102, 7860.